New Journal of Physics
The open access journal for physics

Heavy ion microprobes: a unique tool for bystander research and other radiobiological applications

K O Voss, C Fournier and G Taucher-Scholz[1]
Gesellschaft für Schwerionenforschung (GSI), Planckstrasse 1,
64291 Darmstadt, Germany
E-mail: G.Taucher-Scholz@gsi.de

New Journal of Physics **10** (2008) 075011 (22pp)
Received 18 March 2008
Published 28 July 2008
Online at http://www.njp.org/
doi:10.1088/1367-2630/10/7/075011

Abstract. The risk assessment for low doses of high linear energy transfer (LET) radiation has been challenged by a growing body of experimental evidence showing that non-irradiated bystander cells can receive signals from irradiated cells to elicit a variety of cellular responses. These may be significant for radiation protection but also for radiation therapy using heavy ions. Charged particle microbeams for radiobiological application provide a unique means to address these issues by allowing the precise irradiation of single cells with a counted numbers of ions. Here, we focus specifically on heavy ion microbeam facilities currently in use for biological purposes, describing their technical features and biological results. Typically, ion species up to argon are used for targeted biological irradiation at the vertically collimated microbeam at JAEA (Takasaki, Japan). At the SNAKE microprobe in Munich, mostly oxygen ions have been used in a horizontal focused beam line for cell targeting. At GSI (Darmstadt), a horizontal microprobe with a focused beam for defined targeting using ion species up to uranium is operational. The visualization of DNA damage response proteins relocalizing to defined sites of ion traversal has been accomplished at the three heavy ion microbeam facilities described above and is used to study mechanistic aspects of heavy ion effects. However, bystander studies have constituted the main focus of biological applications. While for cell inactivation and effects on cell cycle progression a response of non-targeted cells has been described at JAEA and GSI, respectively, in part controversial results have been obtained for the induction of DNA damage measured by double-strand formation or at the cytogenetic level. The results emphasize the influence of the

[1] Author to whom any correspondence should be addressed.

cellular environment, and standardization of experimental conditions for cellular studies at different facilities as well as the investigation of bystander effects in tissue will be the aims of future research. At present, the most important conclusion of radiobiology studies at heavy ion microbeams is that bystander responses are not accentuated for increasing ionizing density radiation.

Contents

1. Introduction

Reliable risk estimates for the exposure to densely ionizing components of environmental, cosmic or therapeutically applied radiation are a matter of major concern and there is no controversy about the need for low dose studies using charged particles. While during the past decade the understanding of hazardous biological effects caused by high linear energy transfer (LET) exposure in living organisms has been addressed in a number of studies using light ion microbeam technology [1]–[4], the biological effects of single traversals of heavier particles are not yet fully understood. The increasing application of heavy ions in radiotherapy [5] and also the major contribution of heavy ions to radiation risk in manned space missions [6] point out the importance of addressing these topics. In this context, the development of heavy ion microprobes allowing precise targeting of single cells and subcellular structures has become a primary goal in order to prevent the limitations associated with random hitting of broad beam exposure. The meanwhile available experimental setups for heavy ion cell microirradiation provide a valuable tool to address fundamental radiobiological issues related to radiation protection or radiotherapy.

Important topics in connection with microirradiation technologies are the visualization of DNA damage at a subnuclear scale and the investigation of the spatiotemporal dynamics of DNA damage response processes [7]–[10]. Furthermore, the microbeam technology has been used to analyze the cellular response of non-irradiated 'bystander' cells that are either neighboring irradiated cells or get in contact with the medium of irradiated cells. Up to now, the investigation of differential bystander effects targeting the cell nucleus, the cytoplasm or membranes of single cells has been carried out mainly using light ions, whereas the analysis of the impact of ionization density has also been addressed with heavy ions of different LETs [11, 12].

Herein, a review of the currently available microbeam facilities is presented and relevant technical developments are discussed. In addition, some recent results related to heavy ion biological research are exemplarily highlighted.

2. Charged particle microbeams for cell irradiation

Although the first ion microbeam was used to irradiate biological cells as early as 1953 [13], a veritable rush into this field was triggered in the mid-1990s by the scientific impact of two facilities dedicated to radiobiology at the Gray Cancer Institute (GCI) and at the Radiological Research Accelerator Facility (RARAF). At that time, both were employing collimation either by small pinholes [14] or capillaries [15] to cut a micrometre fraction out of Van de Graaff beams of protons or helium ions. Grossly simplified, the particles coming from below penetrate a dish with cells attached and are detected either in transmission through the dish (RARAF) or by means of a thin beam-transparent scintillator below the dish (GCI); microscopes are used to image the cells from above to individually position target areas in the microbeam, and a fast beamswitch controls the number of particles per target. Meanwhile, many accelerator facilities teamed up with radiobiologists to set up micro-irradiators for single cells.

The basic components of any microbeam, i.e. microbeam formation, cell dish design, particle detection, and beam switching are being implemented in a number of different ways. For microbeam formation, there are the two possibilities of passive beam collimation by means of small apertures or tubes resulting in a stationary microbeam with some scattered particles or ion-optical demagnification of an apertured beam with the potential of smaller beamspot size, a lower fraction of scattered particles reaching the target, and the possibility to position the beam focus on the target by fast electromagnetic deflection. Cell dish design and particle detection are strongly interfering in the sense that any detector transmitted by the ions before they hit the cell dish will have less than perfect efficiency and introduces some ion scattering. Positively, cell dishes used with transmission particle detectors can be allowed to stop the entering particles in a thick layer of culture medium. On the other hand, detectors that fully stop impinging ions may be perfectly efficient and do not introduce scattering, however, they can clearly only be used with ions that have already passed the cell dish. Thus, thin beam-transparent cell compartments with almost no culture medium have to be used.

An overview of the facilities currently in operation or preparation, collimated or focused, dedicated to biology or shared with analytical experiments, has been presented previously [16].

In the following, details are given for the microprobes using ions heavier than helium.

2.1. Heavy-ion single-cell irradiators

As of now, three groups are operating microprobes that use charged particles heavier than helium for radiobiological purposes. Both the microprobe at the Maier–Leibnitz Laboratory in Munich and that of GSI Darmstadt were originally designed for material science applications [31, 32] and have been adapted over the past few years to also suit biological experiments. The system in Takasaki, Japan, on the other hand, started out in the mid-1990 s with biological, though not only single-cell, applications in mind [17]. The main difference between these two approaches is that microprobes dedicated to biology tend to be set up with a vertical end-station in order to connect to a wet sample environment in a natural way. For any horizontal system, this connection is an important design task. An overview of the main technical characteristics of the three heavy-ion microprobes is given in table 1.

It should be mentioned that in addition to the operational heavy-ion microbeams, a source for ions beyond helium is currently under development for the RARAF microbeam in New York [33] and that the new microprobe in Surrey is expected to be able to bend ions as heavy as

Table 1. Main technical characteristics of the three heavy-ion microbeam facilities.

	Ion species	Ion energies	Beamspot size	Targeting accuracy	Ion detection	References
JAEA	He–Ar	~10–20 MeV u^{-1}	$\geqslant 5\,\mu$m	$\geqslant 5\,\mu$m	Scintillation	[17]–[20]
SNAKE	p–Au typically C, O	~4–6 MeV u^{-1}	~550 × 400 nm^2	~2 μm	Scintillation	[21]–[23]
GSI	p-U typically C, Ar, Ni, Pb	1.4–11.4 MeV u^{-1} typically 4.8 MeV u^{-1}	~700 × 500 nm^2	~1.3 μm	Secondary electrons	[24]–[30]

calcium into its vertical beamline [34]. Also some first steps to set up a heavy focused beam for radiobiology have been taken by the accelerator center in Lanzhou, China. Preparations for the installation of a heavy-ion single-cell system were also reported from the Lawrence Berkeley Laboratary [35].

2.1.1. 'SNAKE' microprobe in Munich. The heavy-ion microprobe in Munich is a horizontal system fed by a tandem accelerator that can supply beams from protons to gold ions at voltages up to 14 MV. Typical ion beams used for radiobiology are oxygen and carbon with specific energies around 6 MeV nucleon^{-1}. The beamspot is produced by a superconducting multipole lens in a helium bath that strongly demagnifies the approximately 30 m distant object aperture into the focal plane about half a metre behind the lens. The divergence of the beam entering the lens is limited by a set of microslits some 5 m behind the object aperture. A fast electrostatic beam chopper between object and divergence slits is used to switch the beam with overexposure probabilities in the per mill range at a 1 kHz rate of fast particles [21]. Directly in front of the lens, electrostatic beam deflection is employed to shift the beam in its focal plane.

The focused beam exits the vacuum through a 7.5 μm polyimide foil glued onto an exit nozzle that contains light emitting diodes (LEDs) for phase contrast illumination of the sample. A commercial inverted microscope lying on its side is opposite the exit nozzle and can be aligned relative to the beam with an x–y stage that shifts the entire microscope. The support frame of the microscope is separated from that of the magnetic lens [22]. A miniature photomultiplier tube (PMT) with attached plastic scintillator is situated in one of the objective revolver ports allowing detection of individual particles transmitted through the sample.

The cell dish base is a 6 μm thin Mylar foil carrying the cell layer. As long as it resides in a horizontal position during preparation and incubation, the carrier foil is covered by cell medium. For irradiation, the cell carrier is turned into the vertical with only a thin layer of medium covering the cells in order to allow the ion beam to be transmitted through the sample and to reach the detector. A second Mylar foil closes the cell culture compartment possibly creating a moist atmosphere inside [22]. To reduce the negative effects of malnutrition, the irradiation procedure is limited to 20 min.

Cells are grown on a sheet of plastic scintillator for detection of single ions with scintillation light passing through the optical path of the microscope. The opposite side of the cell compartment is a thin Mylar foil through which the ion beam enters. In between the Mylar and scintillator foils, a thick layer of medium covers the cells to allow for long measurement times. For irradiation of the cells, the Mylar foil is pressed towards the cell bearing scintillator

to reduce the necessary minimum ion range to reach the cells and their scintillator substrate. The beam exit nozzle and the immersion objective as well as the cell stage are heated to 37 °C to reduce cell stress.

In an alternative arrangement specifically designed for *in situ* live cell imaging [36], cells attach to a scintillator platelet through which microscopy observation is performed and are fully immersed in medium inside a large volume heated cell container. This container is closed by a thin Mylar foil. For irradiation, the beam exit nozzle of the microprobe presses onto the Mylar foil until the medium layer covering the cells is less than 30 μm thick and thus transparent to the ion beam. After irradiation, the nozzle is retracted again to allow for a thicker layer of medium and long *in situ* observation time.

The adjustment of the magnetic lens is performed by minimizing the size of the beamspot on a 200 μm thick thallium-doped CsI crystal as it appears in the microscope. As shown by single-ion hit patterns in a track-etch detector [22], this procedure yields small beam foci of around half a micron halfwidth in air. Absolute targeting accuracy has been reported to be roughly 2 μm in a cell culture [23].

2.1.2. JAEA microbeam in Takasaki. One of the Takasaki microbeams is routinely employed for radiobiology using heavy ions [17]. It makes use of heavy-ion species from helium to argon accelerated to specific energies between 10 and 20 MeV nucleon^{-1} by a cyclotron. Passing the beam through a set of two aluminium apertures of 5 mm and 0.5 mm diameter, respectively, performs spatial restriction of the beam. After that, an aligned microaperture with minimum diameter 5 μm cuts out the microbeam. To allow collimation in this way, the thicknesses of the gold or tantalum sheets containing these microapertures have to be greater than the range of the ion beam in that metal. Since the smallest spark-eroded pinholes are seemingly only available in relatively thin metal sheets, long-range particles are collimated to larger beamspots only. Specifically, the finest 5 μm collimation is reported to be available for argon and neon beams below 13 MeV nucleon^{-1}[18].

The microbeam is extracted from the vertical downwards-directed beamline either through a thin plastic foil or directly through the bare collimator opening. Cells and a micrometre thin layer of culture medium are sandwiched between a 100 μm slab of CR39 track detector (bottom) and an 8 μm thin sheet of polyimide through which the microbeam enters. Positions of individual targets relative to fiducial marks imprinted into the CR39 cell substrate are defined in an offline microscope either by manual selection or by automatic recognition of stained cell nuclei [19]. An online inverted microscope determines the position of the fixed beamspot and that of the CR39 fiducial marks. Defined targets can be positioned in the beam using an x–y stage equipped with displacement sensors.

Particles are detected in transmission through the 110 μm sample stack of CR39, cell culture, and polyimide using a scintillator foil directly attached to a miniature PMT. This detector assembly is mounted in one of the objective revolver ports of the online inverted microscope. For irradiation, the objective revolver is switched to the PMT position, the target is moved into the beamspot according to the positional data acquired in the offline microscope. An electrostatic beamswitch between ion source and cyclotron is opened and closed to control the dose on each target.

After irradiation, the bottom surface of the CR39 cell substrate can be etched to reveal positions of particle traversals. Shifting the microscope focal plane from this CR39 bottom surface with etch pits to the top plane with cells, it is possible to evaluate targeting accuracy and

dose distribution, provided the microscope focusing direction is perfectly parallel to the CR39 surface normal. Along these lines, Funayama *et al* recently scored the dose distribution of cells irradiated with five ions each (argon, 11.5 MeV nucleon^{-1}, 5 μm collimator) [18]. They found that about 20% of the targeted cells had been hit by the nominal number of ions. Most cells lacked one or more ions with very few targets receiving no ion hit at all. A few per cent of the cells were overexposed by one or two ions. The authors suggest a number of possible reasons including enhanced scattering in the narrow collimator, uncertainties of target coordinates resulting from sample transfer between the offline microscope to the site of the microbeam, or changes in the live cell culture between target definition and irradiation. Nevertheless, evaluation of the etch pit positions can be used to sort out the received dose for each individual target in retrospect.

Presently, a vertical, downwards-directed heavy-ion microprobe of the focusing type is in the commissioning stage in Takasaki [20].

2.1.3. GSI microprobe in Darmstadt.

2.1.3.1. Beam optics. The GSI heavy-ion microprobe is a horizontal system currently used both as an analytical microprobe for material science in vacuum and as a single-ion cell irradiator for radiobiology with the microbeam extracted into air. The setup employed to form the beam focus for both applications has been described in [24]. Briefly, a triplet of quadrupole magnets images the object aperture into the focal plane with a demagnification of 16× in the vertical and 8× in the horizontal directions. To achieve a small beam focus with this rather low demagnification it is necessary to use a minute object aperture (typically $10 \times 5\ \mu m^2$). Trivially, smaller apertures cause lower particle rate in the experiment and a larger fraction of particles scattered at the edges. While for most ion species low particle rates can be compensated for by very high beam intensities from the accelerator, particle scattering is dealt with by low scattering polished tungsten carbide cylinders with minimum surface roughness forming the object aperture [24]. Further, particles that have been scattered to larger angles and thus spatially separate from the main beam are caught before entering the lens at two sets of anti-scattering slits.

A magnetic beam deflector directly in front of the focusing lens can bend the incoming beam to direct the ion focus to specific places in the focal plane. Supply currents of the deflector can perform a full-scale sweep within a millisecond, which is fast enough for ion rates up to a few hundred hertz when including an additional waiting time to let the magnet settle into each new position.

Fast beam switching is performed by electrostatic deflection plates just in front of the object aperture. Within 200 ns, power amplifiers can charge the opposing plates to +200 V and −200 V, respectively, bending the incoming particle trajectories, so that ions are stopped before entering the magnetic lens. For accurate single-ion switching, the time interval between two particles has to be greater than the time of flight between switch and target plus the time needed to activate the beamswitch. Taking into account the bunched and low duty-cycle nature of our linac beam, acceleration to highest UNILAC velocities, the fast switch, and the short microprobe, the probability of target overexposure due to slow switching is in the per mill range at a 1 kHz particle rate.

To reduce the thermal load on the microslits, properly heat-sinked, micro-controllable tantalum pre-slits are used as entrance aperture to the experiment. Water-cooled slits in front

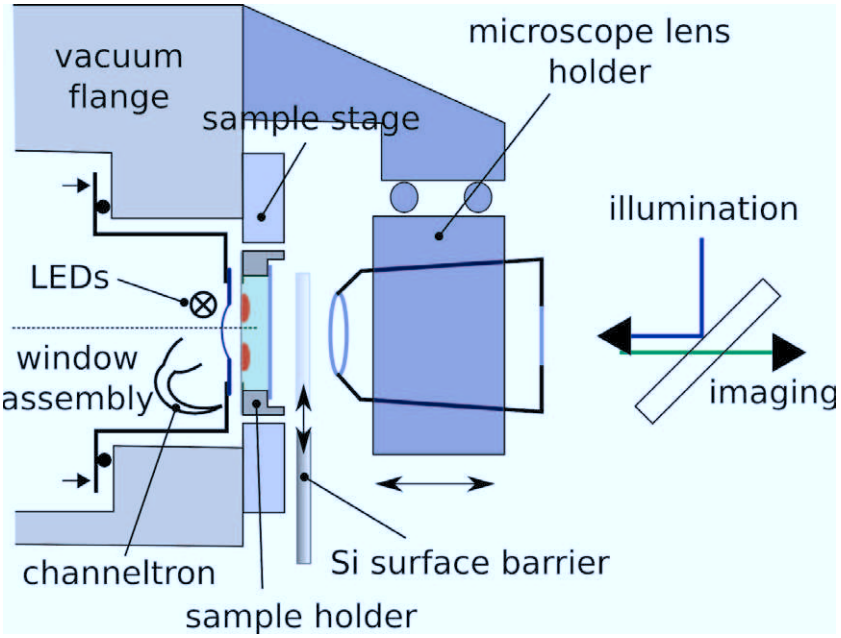

Figure 1. Scheme of the GSI biology microbeam end-station.

of the last bending magnet to the experiment are closed as far as they do not influence the particle rate in the microprobe.

2.1.3.2. Biology end-station. For targeted irradiation of live cells, the ion beam is extracted from the vacuum through a 200 nm thin Si_3N_4 1 mm^2 window (figure 1). The silicon chip carrying the window is glued into position on the window assembly that, in turn, is mounted into the vacuum flange. A compressive rubber ring serves as vacuum-tight seal along with a stack of metal shims used to regulate and minimize the distance between vacuum window and target surface. The window assembly also contains a low noise, high gain electron multiplier to collect and amplify the electron cloud emitted from the vacuum window when a particle passes. Single-ion detection efficiencies close to 1 are reached by optimizing the surface of the window for electron emission. For that purpose, the vacuum side is coated with thin layers of gold and caesium iodide [25, 26]. Along with the electron multiplier, two LEDs are mounted in the window assembly. They can be used for illumination of the sample through the vacuum window.

On the atmosphere side of the window, a dc-motor driven x–y stage with optical displacement sensors forms an integral part of the vacuum flange. Sample holders lock in place very reproducibly in this x–y stage with no significant rotation or tilt. Holders containing live cell cultures comprise a 4 μm thin polypropylene foil with cells attached in a 7.5 mm diameter area, a 0.8 mm thick layer of cell medium, and a microscopy cover glass closing the stainless steel cell dish. Fiducial marks on the foil can be used to revisit individual target points in offline analysis. A long working distance objective is fixed on a short and stable aluminium arm that is tightly coupled to the vacuum flange for enhanced stability. In addition to the LED illumination, light from a high-pressure mercury arc lamp can be used for fluorescence microscopy. For that purpose, it is shaped for Köhler-illumination, color filters can be quickly flipped in and out to switch between different excitation wavelengths, and a fast shutter limits the illumination time

to the necessary minimum. Excitation light is coupled into the objective by a suitable dichroic beam splitter. Fluorescence from the sample passes the splitter, an emission filter, and forms the image on a CCD camera. Targeting coordinates can be generated by computer evaluation allowing for fast, automated irradiation of large numbers of cells.

A silicon surface barrier detector can be flipped into position between sample holder and microscope objective to measure energies of particles transmitted through thin samples.

2.1.3.3. Beam focus. A semi-empirical calculation of lens currents using particle mass, energy and charge state yields settings good enough to produce a beamspot of a few microns. For further beam focusing, the roughly focused beam is scanned over a 12.5 μm period metal grid while recording particle energy and currents of the beam deflector for individual transmitted ions. A scatter plot of x and y deflection currents containing only those particles that have suffered energy loss in the grid bars yields a transmission micrograph of the grid blurred by the imperfect beam focus. The lens currents are then fine tuned until the sharpest transmission micrograph is achieved. So far, the smallest beam focus in air adjusted and measured in this way had halfwidths of 700 nm in x and 500 nm in y directions [27].

2.1.3.4. Calibration of absolute beam position and beam deflection. The position of the beam focus can be detected by an efficient Ce:YAG scintillator mounted in the x–y stage. The microscope objective is adjusted to the position where the scintillation light produced by the undeflected beam is in the center of the microscope field of view. The position of the luminescence maximum on the scintillator is recorded for a set of three x–y pairs of beam deflection currents. From these positions, linear relations for deflection in x and y and the angle spanned by the x-axis of deflection and the x-axis of image formation are derived [28].

Trivially, any change of the elements in the imaging light path introduces the need for recalibration. Only for this reason, both the dichroic beam splitter and the emission filter are locked down statically in the current setup. In the illumination light path, however, excitation filters can be dynamically switched with practically no shift in the microscope image. With this flexibility of excitation wavelength switching, Du *et al* [29] recently used a ratiometric method involving fast switching of two excitation filters to examine the cytoplasmic concentration of free calcium ions in live cells within the first minutes after targeted ion irradiation.

2.1.3.5. Microprobe performance. To judge the capabilities of any single-ion single-cell irradiation setup, one needs to look at a number of different properties: firstly, the size of the beam focus in the target plane is a measure for the precision of ion hits relative to each other. Due to the low scattering power of the thin vacuum window and its minimized distance to the target, the optimum $0.7 \times 0.5\ \mu m^2$ beam focus extracted from the vacuum [27] is just slightly larger than the best beam foci we usually achieve in vacuum with no window scattering at all. Currently, the most probable limiting factor with respect to beam focus size is the chromatic aberration introduced by the energy spread ($>10^{-3}$) of the linac beam. In figure 2, the small sizes of the fluorescence spots immunostained for phosphorylated histone H2AX as well as the regular 3 μm distances of the five spots per cell nucleus demonstrate the high relative precision of our system.

Secondly and more important, the absolute targeting accuracy, i.e. the ability to direct the ion focus into defined targets, strongly depends on the establishment of an error-free calibration putting into relation target points as they are imaged onto the CCD chip of the online microscope

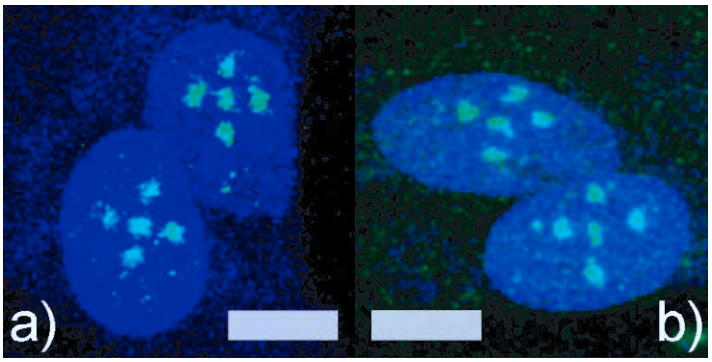

Figure 2. Human fibroblast cell nuclei (blue: ToPro DNA counterstain) irradiated with cross patterns of 20 (a) or 1 (b) carbon ion(s) (4.8 MeV nucleon^{-1}) per spot. Sites of induced DNA damage were visualized by immunostaining of a DNA double-strand break (DSB) marker (green: γH2AX). Spot distance 3 μm, scale bars: 10 μm.

with deflection settings needed to steer the beam to the true, physical position of these target points. To assess the absolute targeting accuracy, the distances of the barycenters of cross patterns like those shown in figure 2 from the barycenter of the cell nuclei that were targeted with the deflected ion microbeam have been evaluated [27, 30]. The average deviation between physical hit and targeted point was found to be about 1.3 μm.

The third measure of performance to look at is dose control. It comprises hit detection efficiency, i.e. the fraction of missed hits and false hit signals, the speed of the beamswitch, and the amount of scattered particles that hit the sample in wrong places. Dose control can easily be checked by writing single-hit patterns into a track-etch detector and counting the numbers of missing, double and misplaced hits. The latest evaluation published for the GSI microprobe found one per mill missing or double hits and four per mill of ions scattered into wrong sites [26].

Another important aspect of a cell irradiator is cell dish design and processing speed. Clearly, the overall biocompatibility of the cell dishes used during irradiation limits the amount of processing time deemed safe with respect to cell 'stress'. Hence, large cell dishes with a large volume of culture medium, controlled atmosphere and well-defined temperature would be favorable. However, especially for a horizontal microprobe, both the size of the culture substrate and the dish volume negatively introduce the need of refocusing the microscope by bending of the thin cell substrate and decrease the achievable targeting accuracy by additional light refraction in the imaging path, respectively. For that reason, our cell compartments are rather small and thin. Thus, typical times we allow the irradiation procedure to take from closing the cell dish to opening it after the experiment range from 15 to 30 min. Usually, about ten fields of view of the online microscope can be irradiated in a 20 min experiment corresponding to about a thousand confluent cells for a 20× objective.

3. Targeted exposure of single cells in radiobiological research

The first experiments aimed at targeted exposure of bacteria spores and mammalian cells to heavy ions were carried out at a collimated GSI microbeam facility almost two decades ago [37]. Since then, the technical developments and the performance of the three heavy ion microbeam

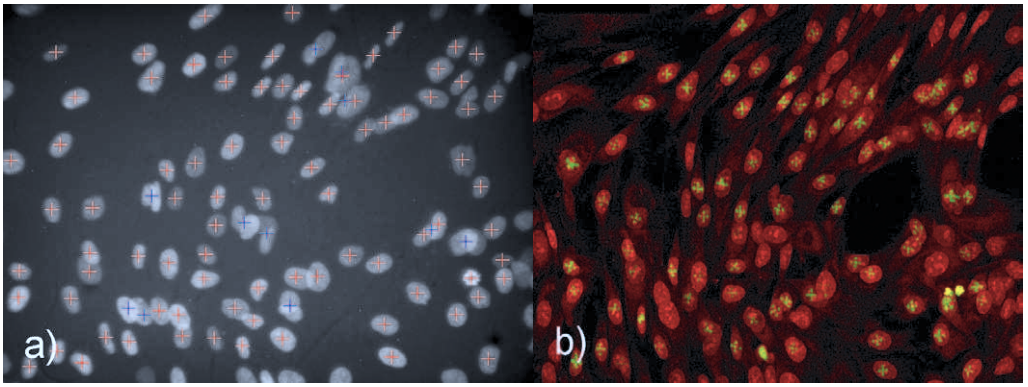

Figure 3. Targeted ion irradiation of single cells. (a) View of the online microscope 20× lens onto a nuclear-stained culture of human fibroblasts with recognized targets prior to irradiation. (b) The same area as seen in an offline microscope after fixation 30 min post-irradiation and immunostaining for γH2AX to visualize DNA damage. DNA counterstained with ToPro. 4.8 eV per nucleon carbon irradiation, 20 ions per spot, 5 spots in cross pattern with 3 μm distances.

facilities described above have provided powerful tools that are currently being used in several fields of life science research, i.e. for radiobiological purposes. Modern technologies for the visualization of DNA lesions based on immunofluorescence microscopy (in fixed or living cells) perfectly add on the possibilities to produce defined distributions of localized DNA damage using microbeams, as outlined in section 3.1 below. However, the main advantage of microbeam application arises from the opportunity to specifically irradiate single cells within a cell population (figure 3), and to assess a wide spectrum of radiation-induced cellular responses differentially in targeted and nearby non-targeted bystander cells. Consequently, cellular bystander effects are among the most extensively studied end points in the field of microbeam radiobiology and will be extensively discussed focusing on mammalian cells in section 3.2. In addition, the aimed irradiation of subcellular compartments is briefly addressed in section 3.3.

Beside the purposes of investigation described below, the collimated heavy ion microbeam developed at JAEA has been used for the exploration of radiation-induced effects on targeted regions in multicellular animal and plant models. These topics have been extensively described recently and will not be further addressed here [38]. Recent reports are focused on tobacco plants [39], insect developmental biology investigated in the silkworm *Bombyx mori* and silkworm larvae [40, 41] and positional radiation effects in nematode germline cells of *Caenorhabditis elegans* [42].

In the following sections, the state-of-the-art regarding heavy ion microirradiation effects in mammalian cells is discussed in the context of providing new perspectives to answer open questions in radiobiology.

3.1. Visualization of DNA damage and recruitment of repair proteins

The specific physical properties of low energy charged particle broad beams have been used to create locally restricted sites of subnuclear damage allowing for a subsequent analysis of the time, but also in particular of the spatial aspects of the DNA damage recognition and repair

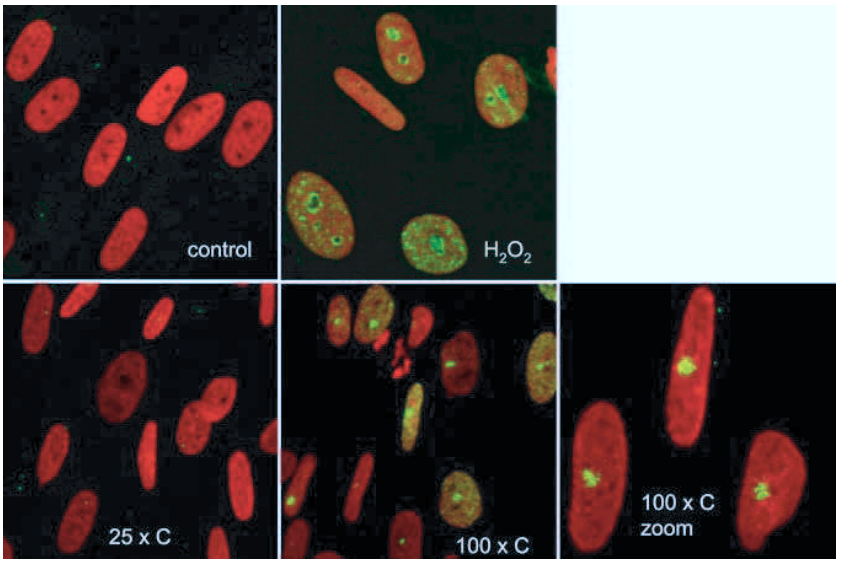

Figure 4. Detection of PAR synthesis at DNA damage sites. The cells were either mock-treated, H_2O_2-treated or targeted with 25 or 100 nuclear traversals of carbon ions (LET 300 keV μm^{-1}). H_2O_2-treatment (5 mM/10 min) results in detectable foci of PAR that are distributed in a granular pattern all over the nucleus. The formation of bright and large PAR-foci at the sites of nuclear traversals was observed when a high number of ions was delivered at one position (100 traversals = 20 Gy). Fixation and staining was performed based on the method described in [48] and confocal microscopy was used for analysis as reported previously [49]. Courtesy of B Jakob.

processes (for review see [10]). However, randomly occurring ion traversals constitute a limiting factor in these studies that can be circumvented by the use of microbeams.

As a first step in the aimed single cell irradiation by means of the GSI microbeam, nuclear DNA damage was visualized after targeting the nuclei of skin fibroblasts with carbon and argon ions (LET 300 and 1950 keV μm^{-1}, respectively) and subsequent immunostaining of 53BP1 (p53-binding protein 1) [27]. One of the main focuses of the radiobiological research activities at GSI is the recruitment of repair proteins to damaged sites of the DNA and the associated modification of some of these proteins. In this regard, the catalytic activity of poly (ADP-ribose) polymerases (PARPs) that are immediately stimulated by DNA strand breaks [43, 44] is of interest. As the involvement of this group of enzymes in the cellular response to DNA damage has been suggested, the transfer of the poly ADP-ribose (PAR) moieties to nuclear proteins was assessed at the Gray Cancer Institute microbeam targeting the nuclei of human tumor and rodent cells with 3.2 MeV protons at doses ranging between 5 and 20 Gy [45]. The results revealed an immediate and dose-dependent PAR signal at the sites of local irradiation, together with a coincident recruitment of the ATM and RAD51 proteins. In contrast, after broad beam irradiation with uranium ions at GSI, a PAR signal at the sites of ion traversal (each corresponding to 10 Gy) was not detected (not shown), in contrast to the positive PAR signal obtained after H_2O_2 treatment (figure 4). Given that ADP-ribosylation is clearly associated with single-strand break (SSB) repair [46] the question arose whether a higher density of DSBs

relative to SSBs induced by the very densely ionizing uranium ions [47] could be the reason for this apparent discrepancy. A microbeam experiment at GSI allowed targeting the cell nuclei with similar doses of intermediate LET carbon ions (LET 300 keV μm^{-1}), showing that 25 hits did not result in a positive staining for PAR at the damaged site, whereas a 4-fold higher number of hits delivered to one position in the nucleus showed a bright focus at the damaged site (see figure 4). The number of traversals delivered corresponded to 5 and 20 Gy, respectively, suggesting that only the higher, locally deposited dose resulted in a detectable signal of the ADP-ribose moiety. Besides the shift of the detection threshold to a slightly higher dose, this is in agreement with the previous observation by Tartier *et al* [45] and points to differential effects with respect to PARP activities depending not only on dose but also on the ionizing density and damage quality of the nuclear hits.

In another approach, using the SNAKE microbeam in Munich, human tumor HeLa cells were targeted with oxygen ions (6.3 MeV u^{-1}) in a geometrical irradiation pattern. The accumulation of the repair protein RAD51 was used as a biological track detector after irradiation, confirming the accumulation of RAD51 at damaged sites [22]. In order to test the simple model of homogeneous chromatin distribution, HeLa cells were irradiated with 29 MeV lithium ions and 24 MeV carbon ions. Based on the obtained results, the authors postulate that the observed 53BP1 distribution along the tracks is not reconcilable with this simple assumption and suggest that the biological track structure is determined by cell nuclear architecture with higher order organization of chromatin [50], confirming previous observations obtained using statistical low angle irradiation [51].

3.2. Bystander effects

The biological efficiencies of low doses are not clear up to now, in that increased and also decreased sensitivities of cells upon low dose exposure are reported [1]. For charged particle irradiation the delivery of low doses implies always that single cells of a monolayer or a tissue receive a high dose, whereas adjacent, so-called 'bystander cells' are not irradiated. Therefore, in the case of particles, the controversial discussion about the eligibility of a linear extrapolation of dose response curves to low doses is closely related to the question of whether bystander cells exhibit cellular responses that are generally attributed to irradiation. Most of the bystander studies have been carried out either using low LET irradiation (medium transfer or co-culture experiments) or, when high LET-induced effects were studied, exposing the cells to a counted number of helium ions or to low fluences of α-particles. Up to now radiation-induced bystander effects have been reported for a large variety of cellular effects, including changes in cell cycle progression and regulation, DNA and cytogenetic damage, gene mutations, altered survival and cell death. In view of these results, the existence of extranuclear targets of irradiation has been proposed [4], [52]–[54].

The exploration of the underlying mechanisms has brought up essentially two basic ideas. One is that soluble factors are released by irradiated cells, triggering bystander responses via diffusion in cells sharing the surrounding medium with the irradiated cells [55]–[57]. In order to test for the proposed involvement of soluble factors, either co-culture systems are being used, or the supernatant of irradiated cells is transferred to unirradiated cells. The other hypothesis is that signal transmission from irradiated to bystander cells is mediated via gap junctions that are established between adjacent cells [58]. Based on this idea, the assessment of bystander effects mediated by cell-to-cell communication has to be carried out in cell monolayers and, as

a consequence, it is important to discriminate between the irradiated and bystander cells. For this purpose, microbeams are an excellent tool, combining high LET irradiation with precise targeting of single cells. The following compilation of bystander responses focuses on those cellular effects investigated after heavy ion exposure.

3.2.1. Cell cycle related effects. We could previously demonstrate cell cycle related bystander responses in skin fibroblasts using either broad beams of carbon or of uranium ions (LET 11–15 000 keV μm^{-1}), both after low fluence irradiation and by co-culturing irradiated and bystander cells [59]. As the obtained results suggest at least in part soluble factors to be responsible for the observed effect, we addressed whether the responding bystander cells were located adjacent to the hit cells, hypothesizing that also gap junction mediated signal transmission could be involved. We targeted single cells with carbon ions (LET 310 keV μm^{-1}) and quantified after immunofluorescence staining the overall induction of CDKN1A (formerly known as p21) in nuclei in proximity to the hit cells. No relationship was found between the accumulation of CDKN1A and the radial distance to the irradiated cells [59]. In a further step, we extended the investigation to ions with higher LET. Targeting single cells with argon ions (LET 1950 keV μm^{-1}) and quantifying the protein accumulation in about 10 radial image fields around each of the irradiated cells (each field containing on average 30–35 cells) showed no evidence of the appearance of clusters of bystander cells with a radiation-induced enhanced level of CDKN1A (figure 5). On the other hand, a small bystander effect can be inferred when comparing the level of p21 in the overall population of non-targeted cells with control cells of separate, mock irradiated chambers. Thus, at a higher LET we can confirm the lack of correlation between the magnitude of the CDKN1A induction in bystander cells and their distance from the targeted cells. It should be noted that using a more reliable method, where control and bystander cells were in the same chamber but were separated during irradiation by a stick which was removed for immunostaining in order to control for staining variations, a small bystander effect of the same range was also observed for carbon ion exposure [59].

3.2.2. DNA damage in bystander cells. The cell cycle related changes observed in fibroblast bystander cells motivated us to assess DNA damage that has been hypothesized to be one of the triggering events for cellular bystander effects [60]. However, in a systematic study using proliferating human fibroblasts we found no evidence for the bystander formation of γH2AX foci at 18 h post-irradiation when we used carbon ions (LET 170 keV μm^{-1}) to target single fibroblast cells [59].

Exemplarily, the distribution of γH2AX foci in mock exposed controls and bystander cells is shown in figures 6(a) and (b). The number of cells containing an excess number of foci (> mean value in control cells +1.5 standard deviations) for the samples shown was 11% in controls versus 9.5% in bystander cells. An increase in the LET of the radiation was achieved using nickel ions (LET 3800 keV μm^{-1}) under the same experimental conditions (18 h). The obtained values for the number of cells containing an exceeding number of γH2AX foci versus the respective control was 11.7, indicating no effect of the enhanced LET. On the other hand, using nickel ions the bystander response of a confluent fibroblast population was tested. The corresponding distribution of γH2AX foci in controls and bystander populations at 12 h post-irradiation is depicted in figures 6(c) and (d). Lower mean values (1.6/1.8 in confluent cells versus 5.1/4.8 in proliferating cells) were obtained and attributed to the lower number of S-phase cells containing replication-induced γH2AX foci, but the fraction of cells with an

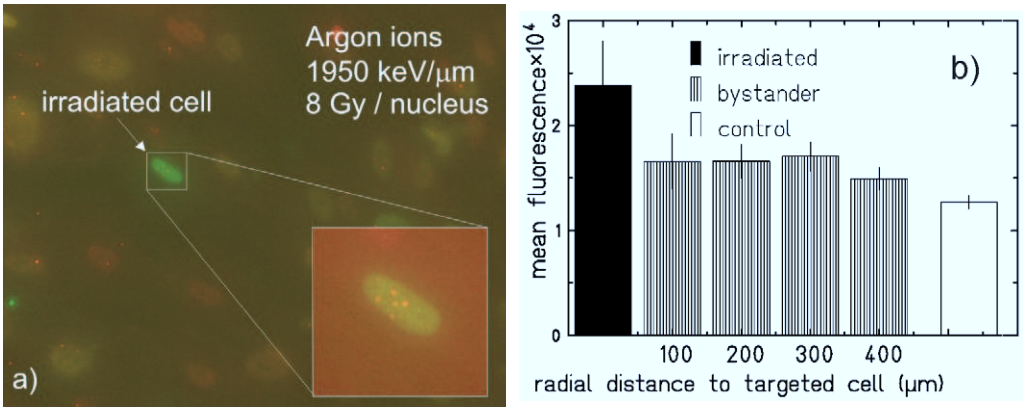

Figure 5. Mean CDKN1A fluorescence intensity as a function of radial distance to single cells targeted with argon ions. For each of the four chambers 10 image fields (each containing on average 30–35 cells) were evaluated revealing comparable results, shown here for one representative sample. (a) Single cells were targeted with 5 hits of argon ions in a cross formation. The hits were visualized by γH2AX immunofluorescence staining (see enlarged inset). (b) After the identification of the irradiated cells by coordinates, virtual rings with increasing distance to the irradiated cells (as indicated) were drawn and the CDKN1A levels in bystander cells were analyzed separately for each virtual ring. Up to the radial distance of 400 μm the CDKN1A protein amount per nucleus did not change significantly and revealed no clusters of cells bearing an increased CDKN1A protein level. The experimental procedure has been described previously [59]. Briefly, protein was quantified by immunofluorescence staining of the adherent cells using: anti-CDKN1A (mouse, Transduction laboratories), anti-γH2AX Ser-139 (rabbit, Upstate, USA) and secondary Alexa Fluor 488- and Alexa Fluor 568-conjugated antibodies. DAPI was used for counterstaining of cell nuclei. Images were acquired using a fluorescence microscope (DM, IRBE, Leica, Wetzlar, Germany) and images were processed for using ImageJ (NIH, Bethesda, MD).

excess number of foci did not change in the bystander sample and is similar to the value obtained in the proliferating cells (12.3% in controls versus 11.8% in bystander cells).

In contrast to our results suggesting that even an increased LET compared to carbon ions does not lead to a detectable effect, an excess number of γH2AX bystander foci was detected by Yang *et al* [57] after co-culture of the same cell line with cells exposed to high energy iron ions (LET 151 keV μm^{-1}). Also α-particles have been shown to induce an excess number of γH2AX foci in bystander cells [61, 62]; similar results were obtained after co-culturing bystander cells and cells irradiated with x-rays [56, 57]. The reasons for these divergences are yet to be elucidated but may be related to the differences in the energies of the radiation qualities, the ratio between irradiated and bystander cells or unavoidable minor differences in cell growth and culture conditions as discussed below.

DNA damage, i.e. DSBs may result in the formation of micronuclei, a widely used marker of cytogenetic damage [63]. The formation of micronuclei in bystander cells has been assessed following exposure to various radiation qualities. An enhanced bystander formation has been

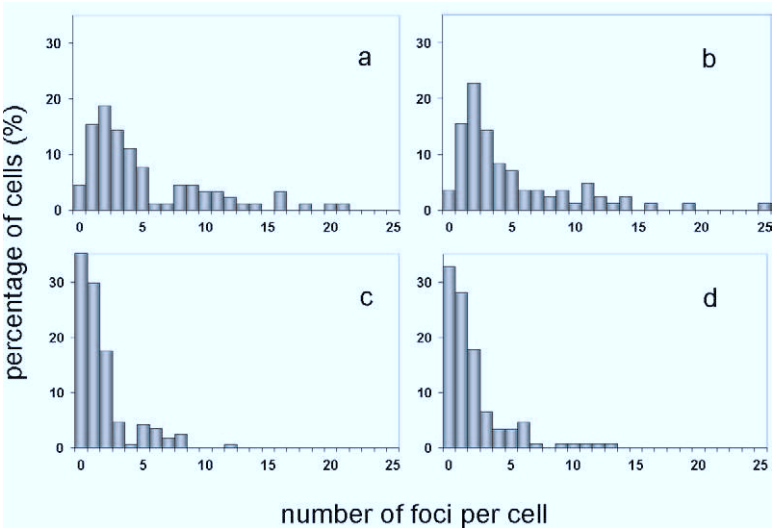

Figure 6. Percentage of cells containing an excess number of foci in control and bystander cells at 18 h after exposure to carbon (controls (a), bystander (b)) and 12 h after exposure to nickel ions (controls (c), bystander (d)). Visualization of γH2AX foci by confocal laser microscopy after immunofluorescence staining was performed as described elsewhere [51], but without extraction procedure. The identification of γH2AX foci was performed by a semi-automatic threshold intensity evaluation based on Image Pro Plus. After obtaining a distribution of cells with the counted numbers of foci per cell, the fraction of cells with an excess number of foci above a threshold defined as the mean number of foci in control cells +1.5 standard deviations was determined. Courtesy of P Barberet.

mainly reported following exposure to sparsely ionizing irradiation (co-culture and medium transfer experiments) [56], low fluences of α-particles [64, 65] and after targeting single cells with helium ions [66, 67]. In contrast, using the ultrasoft x-ray microbeam of the Gray Cancer Institute, a bystander formation of micronuclei was only detected in repair deficient, but not in wild type rodent cells [68]. For heavy ions, contradictory indications are apparent from experiments exposing skin fibroblasts to broad beams of heavy ions. A bystander formation of micronuclei has been reported after co-culture with carbon [69] and iron ion irradiated cells [57]. Similar results were reported after targeting of less than 0.01% of the cells of the same cell strain with argon and neon ions using the JAEA microprobe [69]. However, our own results obtained by exposure to low fluences did not provide evidence for a bystander effect (carbon, LET 170 keV μm^{-1}; uranium, LET 15 000 keV μm^{-1}). This was corroborated after targeting of 1 and 3% of the cells with carbon ions using the GSI microprobe (LET 300 keV μm^{-1}) or the JAEA microprobe in a comparable experiment [59]. Besides the difference in the percentage of irradiated cells, we hypothesize that the divergences between our results and the published data arise from unavoidable differences between nutrient supply, cell history (freezing, thawing, etc) and other factors which might interfere with a potential bystander response regarding the responsiveness of bystander cells or the magnitude of the effect.

3.2.3. Clonogenic survival. Potential DNA and cytogenetic damage can be expected to lead not only to an inhibition of the cell cycle progression as discussed above, but also to reduced survival. Although we observed after exposure to low fluences an inhibition of the cell cycle, this effect was transient and two weeks after exposure no enhanced transition from mitotically active to postmitotic cell stages in bystander cells was observed [59]. This behavior is not supportive of a decrease in survival. In contrast, for the targeted exposure to less than 0.01% of the cells of the same cell strain with 10 ions reduced survival and small effects regarding a transient apoptotic response and delayed p53 phosphorylation were reported [70]. Comparable effects were observed in CHO bystander cells after targeted exposure to argon ions (LET 1260 keV μm^{-1}), but for carbon ions (LET 120 keV μm^{-1}) in germlines nematode cells only small, if any reductions in the proliferation activity were found [71]. Using a high-LET ultrasoft x-ray microbeam, a reduction of the clonogenic survival was found in rodent cells [72].

3.2.4. The role of gap junctions in high-LET-induced bystander effects. The fact that no clusters of cells highly expressing the CDKN1A protein have been found argues against the hypothesis of gap junction mediated signal transmission to the bystander cells, but it can alternatively be assumed that a fraction of the bystander cells are 'non-responders'. Additional experiments showed that after heavy ion exposure the participation of gap junctions in the signal transmission is more complex than expected from the results reported for α-particles, where the signal transmission via gap junctions was tested by dye transfer and an induction of the structure protein connexin 43 was shown after exposure to low fluences [73].

Nevertheless, we could confirm the effective operation of gap junctions in the cell strain used also by a dye transfer assay (figure 7(a)). This functionality was independent of a previous exposure to broad beams of carbon and uranium ions (not shown). In addition, connexin 43 was only induced after irradiation with high fluences of carbon ions, but not after low fluence exposure (1–10% of the cell nuclei hit) (figure 7(b)). Up to now no data on the functional operating of gap junctions under microbeam conditions are available, although this seems important in order to assess the basis of the differences between the observations after low fluences of α-particles and carbon ions.

The functionality of gap junctions can only be inferred indirectly from data on the bystander induction of micronuclei that was reduced in the presence of gap junction inhibitors. This was reported after targeted irradiation of 0.02% of skin fibroblast population with neon (LET 375 keV μm^{-1}) and argon ions (LET 1260 keV μm^{-1}) [69].

3.2.5. Dependence of bystander effects on LET and experimental parameters. For the direct exposure of cells to heavy ions, various cellular reactions have been reported to show a specific high LET pattern, comprising clonogenic survival [74], DNA damage repair [75]–[77]; chromosomal aberrations [78, 79] and cell cycle delay [80]. In general, the direct biological effects are ascribed to the increased ionizing density of ion tracks and the production of complex DNA damage in consequence of the high local deposition of dose [81, 82]. As a result of the formation of a more severe, clustered type of lesions that are difficult to repair, an increased efficiency for various cellular end points like cell inactivation and cell cycle arrest is observed. However, it is still an open question whether the occurrence or the magnitude of bystander effects depends on the ionizing density of radiation. Based on the observation of a transient cell cycle inhibition and similar results for heavy ions of a very broad LET range, we concluded

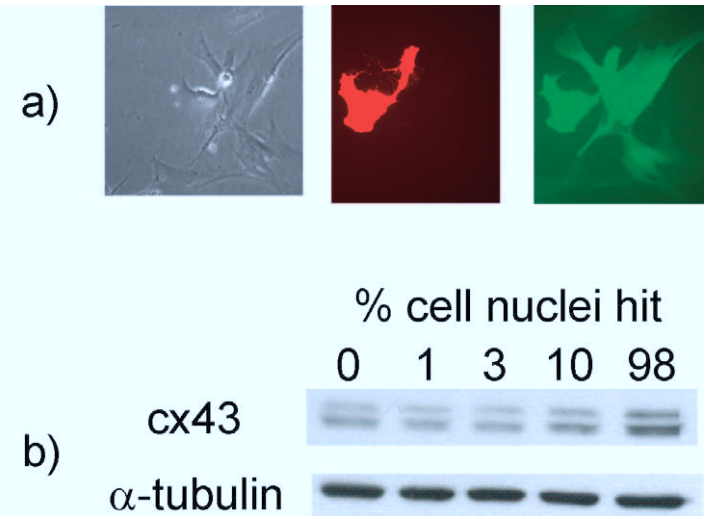

Figure 7. (a) Functionality of gap junctions in AG1522 cells: transfer of the fluorescent dyes DiI and Calcein AM (Molecular Probes). Confluent cells (mock-irradiated or irradiated) were stained, harvested and seeded at a low density on a nearly confluent monolayer of cells of the same strain. Dye transfer was observed during 4 h microscopically. Dye transfer was detected from 2 h after seeding, irrespective of preceding irradiation with x-rays or carbon ions. (b) Expression of connexin43 after carbon ion exposure: representative Western blots showing the expression of connexin43 3 h after exposure to carbon ions in AG1522 cells (two experiments). The fluences were chosen in order to irradiate between 1 and 98% of the population. The different bands of connexin43 correspond to the native and the phosphorylated forms of the protein. α-tubulin was used as a control for equal protein loading. Cells were kept under standard culture conditions before harvest.

that the cellular response in bystander cells is not increased with LET [59]. Bystander responses independent of the LET were also found by Shao *et al* [69] and Hamada *et al* [70].

In addition, we hypothesized that a homogeneous intracellular dose distribution might be favorable for the transmission of bystander soluble signal molecules [59]. This is in line with data comparing x-ray and iron- or neon-ion induced signal transmission via soluble factors [57, 83].

However, in contrast to published data, our recent results revealed no detectable DNA and cytogenetic damage in bystander cells for low and high LET exposure, suggesting that factors other than radiation type may interfere with potential bystander effects [84]. The evidence for this was provided by an experiment performed in parallel at two microbeam facilities (GSI, JAEA). We suggest that unavoidable minor differences in nutrient supply, i.e. the batch of the fetal calf serum, may contribute to the variations in the bystander behavior of cells. Supportive for this is a study revealing a strong influence of the fetal calf serum on the yield of chromosomal aberrations [85].

The technical requirements on the design of microbeam facilities are to some extent antagonistic to an optimal environment for living cells. For example, the thickness of the cell support has to be chosen according to the penetration depth of the ions and the material of the support according to its optical qualities. But the support also has a large impact on the

general cellular stress response, potentially interfering with a radiation or a bystander response. One example is the manifestation of DNA damage in terms of the formation of γH2AX foci. We observed that the average number of foci in skin fibroblasts was about 2-fold higher when they were grown on polypropylene foil (used at the GSI microbeam facility) compared to plastic cell culture dishes. A similar difference can be inferred from the results on glass slides versus polypropylene foil reported by Sokolov *et al* [62]. For cytogenetic damage an influence of the support is also observed, shown for preirradiated cell culture surfaces [64].

Another important point is the UV exposure for the recognition of the cell nuclei after nuclear staining [86]. In the current protocol used for the experiments at the GSI facility, the working dilution of the nuclear dye and the intensity and time of UV illumination (371 nm) have been optimized in order to allow for a clear recognition of the cell nuclei and at the same time to spare the cells from additional DNA damage. The concentration of the nuclear dye (50–100 nM Hoechst) has been lowered such that in a serial test of mock irradiated control dishes using different intensities of UV exposure (usually below 1 kJ m^{-2}), no significant difference in the induction of γH2AX foci was observed comparing the lowest intensity with a 3-fold elevated intensity of UV light.

3.3. Differential subcellular targeting

Advantage from microbeam targeting is taken in the investigation of differential effects when the cell nucleus or the cytoplasm is traversed by particles. Delivering single argon ions (LET 1260 keV μm^{-1}) to the cytoplasm or the nucleus of rodent cells, as determined by retrospective etching of the sites of ion traversal, showed that for both, cell growth was significantly suppressed [71]. In another work the cytoplasm of HeLa tumor cells, wild type and mitochondrial function deficient mutants, were targeted with helium ions, revealing that an active mitochondrial function is required for the bystander response, based on the observation of the relocalization of 53BP1 as a marker for DNA damage [87].

A further purpose is the investigation of the influence on the cytoplasmatic signal transduction. Calcium signaling is part of the immediate stress response of cells to a large variety of insults. A transient increase of intracellular calcium has been reported after exposure of human cells to ionizing radiation [88]. The onset of calcium signaling after heavy ion irradiation was investigated by fluorescence microscopy ratio imaging using the fluorescent indicator fura-2 to measure changes in the level of intracellular free calcium ions. Taking advantage of the high precision of the GSI microprobe, skin fibroblasts were targeted in the nucleus and the cytoplasm separately with carbon and argon ions (4.8 MeV u^{-1}) and the targeted cells were observed in real time during the radiation exposure. However, no radiation induced increase of the intracellular level of calcium was detected, regardless whether the cytoplasm or the nucleus was traversed by a particle [29].

Microbeam irradiation can also be used for the investigation of radiation sequela in subcytoplasmatic structures. Changes in the cellular architecture were recently reported by targeting microfilaments with neon and argon ions (LET 375–1260 keV μm^{-1}) [89].

4. Summary and perspectives

The biological effects of single particle traversal are of practical concern for radiation protection but are not yet fully understood. Charged particle microbeams provide a unique tool for the

defined targeting of single cells. In the past few years many charged particle microbeam facilities for radiobiology have come into operation or are under development worldwide. Herein, the currently available heavy ion microbeam facilities are described in relation to technical achievements and recent biological applications.

In radiobiology research radiation-induced bystander effects have become a well-established phenomenon observed across a variety of end points for both high and low LET radiations. The benefits of precisely irradiating single cells with heavy ions ($Z >$ helium) to study bystander responses as a function of high-LET radiation quality are emphasized here. In spite of the availability of these unique tools, the biological effects observed in bystander cells following heavy ion exposure are still under debate. For normal human cells, conflicting results are reported with respect to the induction of DNA or cytogenetic damage in bystander cells. To reconcile these data it seems appropriate to control for potential experimental variations like the cell strains used and the precise culture conditions, but also to compare experiments with the same protocols at different facilities. On the other hand, the published data on cell cycle effects in bystander cells are in accordance, demonstrating a transient inhibition of the cell cycle progression as reflected by the induction of cell cycle inhibiting proteins. Regarding cell inactivation, the data presently available show an enhancement of apoptosis and a reduction of clonogenic survival in human and rodent bystander cells, indications for the latter have also been reported by co-culture experiments. In contrast, for premature differentiation, which is related to clonogenic survival, no bystander effects were found up to now in low fluence experiments. Clearly, the most important finding supported by the majority of the heavy ion studies available is that in contrast to many direct effects, bystander responses do not seem to be accentuated with increasing ionizing density radiation. In view of the apparent impact of non-assessable factors on *in vitro* cell systems, the goal of future studies should be the investigation of heavy ion effects in tissue models, as recently reported for alpha-particles and helium ions [90, 91].

The opportunity to deposit defined particle numbers on a subcellular or even subnuclear level represents a further gain of radiobiological studies using the heavy ion microprobe. The aimed irradiation enables the analysis of DNA damage and associated cellular responses on a cell-by-cell basis. Future developments aimed at combining the heavy ion microprobe technologies with emerging live-cell imaging approaches [8, 92] should provide an unprecedented stimulus to charged particle radiobiology research.

Overall, the gained insights will help elucidate the mechanism(s) surrounding high-LET DNA damage response and bystander signal production and allow the assessment of eventual consequences in space radiation risk or medical application.

Acknowledgments

We are grateful to Burkhard Jakob and Philippe Barberet for providing unpublished data. We are greatly indebted to Bernd Fischer for a critical reading of the manuscript and for helpful discussions. We thank Bernd Fischer and Markus Heiß for their excellent support at the GSI microprobe and Gerhard Kraft and R Neumann for their continuous support of the microbeam research at GSI.

References

[1] Brenner D J *et al* 2003 *Proc. Natl Acad. Sci. USA* **100** 13761–6
[2] Hall E J 2003 *Health Phys.* **85** 31–35

[3] Prise K M, Folkard M and Michael B D 2003 *Radiat. Prot. Dosim.* **104** 347–55
[4] Prise K M, Schettino G, Folkard M and Held K D 2005 *Lancet Oncol.* **6** 520–8
[5] Schulz-Ertner D and Tsujii H 2007 *J. Clin. Oncol.* **25** 953–64
[6] Cucinotta F A and Durante M 2006 *Lancet Oncol.* **7** 431–5
[7] Essers J, Vermeulen W and Houtsmuller A B 2006 *Curr. Opin. Cell Biol.* **18** 240–6
[8] Lukas C, Bartek J and Lukas J 2005 *Chromosoma* **114** 146–54
[9] Friedl A A 2007 The role of chromatin structure and nuclear architecture in the cellular response to DNA double-strand breaks *Genome Integrity: Facets and Perspectives* ed D-H Lankenau (Berlin: Springer)
[10] Taucher-Scholz G and Jakob B 2007 Ion irradiation as a tool to reveal the spatiotemporal dynamics of DNA damage response processes *Genome Integrity: Facets and Perspectives* ed D-H Lankenau (Berlin: Springer)
[11] Hamada N, Matsumoto H, Hara T and Kobayashi Y 2007 *J. Radiat. Res.* **48** 87–95
[12] Prise K M, Folkard M, Kuosaite V, Tartier L, Zyuzikov N and Shao C 2006 *Mutat. Res.* **597** 1–4
[13] Zirkle R E and Bloom W 1953 *Science* **117** 487–93
[14] Randers-Pehrson G, Geard C R, Johnson G, Elliston C D and Brenner D J 2001 *Radiat. Res.* **156** 210–4
[15] Folkard M, Vojnovic B, Hollis K J, Bowey A G, Watts S J, Schettino G, Prise K M and Michael B D 1997 *Int. J. Radiat. Biol.* **72** 387–95
[16] Gerardi S 2006 *Radiat. Prot. Dosim.* **122** 285–91
[17] Watanabe H and Sudo Y 2003 *Nucl. Instrum. Methods* B **210** 1–5
[18] Funayama T *et al* 2008 *J. Radiat. Res.* **49** 71–82
[19] Kobayashi Y, Funayama T, Wada S, Taguchi M and Watanabe H 2003 *Nucl. Instrum. Methods* B **210** 308–11
[20] Oikawa M, Satoh T, Sakai T, Miyawaki N, Kashiwagi H, Kurashima S, Okumura S, Fukuda M, Yokota W and Kamiya T 2007 *Nucl. Instrum. Methods* B **260** 85–90
[21] Hauptner A 2006 *Dissertation* Technical University, Munich
[22] Hauptner A, Dietzel S, Drexler G A, Reichart P, Krucken R, Cremer T, Friedl A A and Dollinger G 2004 *Radiat. Environ. Biophys.* **42** 237–45
[23] Dollinger G *et al* 2006 *Nucl. Instrum. Methods* B **249** 270–7
[24] Fischer B E 1985 *Nucl. Instrum. Methods* B **10/11** 693–6
[25] Fischer B E, Cholewa M and Noguchi H 2001 *Nucl. Instrum. Methods* B **181** 60–5
[26] Fischer B E, Heiss M and Cholewa M 2003 *Nucl. Instrum. Methods* B **210** 285–91
[27] Heiß M, Fischer B E, Jakob B, Fournier C, Becker G and Taucher-Scholz G 2006 *Radiat. Res.* **165** 231–9
[28] Heiß M 2004 *Dissertation* Technical University Darmstadt
[29] Du G, Fischer B E, Voss K-O, Becker G, Taucher-Scholz G, Kraft G and Thiel G 2008 *Radiat. Res.* at press
[30] Barberet P, Heiß M, Du G, Fischer B E and Taucher-Scholz G 2006 *Acta Phys. Pol.* A **109** 329
[31] Hinderer G, Dollinger G, Datzmann G and Körner H J 1997 *Nucl. Instrum. Methods* B **130** 51–6
[32] Fischer B E 1988 *Nucl. Instrum. Methods* B **30** 284–8
[33] Bigelow A W, Randers-Pehrson G, Kelly R P and Brenner J 2005 *Nucl. Instrum. Methods* B **241** 874–9
[34] Kirkby K J, Grime G W, Webb R P, Folkard M, Prise K and Vojnovic B 2007 *Nucl. Instrum. Methods* B **260** 97–100
[35] Schenkel T, Reijonen J, Persaud A, Kraemer A, Leung K N, Gough R A, Barletta W A and Blakely E A 2002 *Radiat. Res.* **158** 368
[36] Reichart P, Greubel G, Hable V, Hartung P, Hauptner A and Dollinger G 2007 *Maier-Leibnitz Laboratory Anual Report 85* Available online at http://www.bl.physik.tu-muenchen.de/bl_rep/jb2007/p085.pdf
[37] Kraske F, Ritter S, Scholz M, Schneider M, Kraft G, Weisbrod U and Kankeleit E 1990 *Radiat. Prot. Dosim.* **31** 315–8
[38] Kobayashi Y *et al* 2004 *Biol. Sci. Space* **18** 235–40
[39] Yokota Y, Yamada S, Hase Y, Shikazono N, Narumi I, Tanaka A and Inoue M 2007 *Radiat. Res.* **167** 94–101
[40] Fukamoto K *et al* 2007 *J. Radiat. Res.* **48** 247–53
[41] Kiguchi K, Shirai K, Kanekatsu R, Kobayashi Y, Tu Z L, Funayama T and Watanabe H 2003 *Nucl. Instrum. Methods* B **210** 312–5

[42] Sugimoto T, Dazai K, Sakashita T, Funayama T, Wada S, Hamada N, Kakizaki T, Kobayashi Y and Higashitani A 2006 *Int. J. Radiat. Biol.* **82** 31–8
[43] Amé J C, Spenlehauer C and de Murcia G 2004 *Bioessays* **26** 882–93
[44] Schreiber V, Amé J C, Dolle P, Schultz I, Rinaldi B, Fraulob V, Menissier-de Murcia J and de Murcia G 2002 *J. Biol. Chem.* **277** 23028–36
[45] Tartier L, Spenlehauer C, Newman H C, Folkard M, Prise K M, Michael B D, Menissier-de Murcia J and de Murcia G 2003 *Mutagenesis* **18** 411–6
[46] Dianov G L and Parsons J L 2007 *DNA Repair* **6** 454–60
[47] Taucher-Scholz G and Kraft G 1999 *Radiat. Res.* **151** 595–604
[48] Bürkle A, Chen G, Kupper J H, Grube K and Zeller W J 1993 *Carcinogenesis* **14** 559–61
[49] Jakob B, Scholz M and Taucher-Scholz G 2000 *Radiat. Res.* **154** 398–405
[50] Hauptner A *et al* 2006 *Radiat. Prot. Dosim.* **122** 147–9
[51] Jakob B, Scholz M and Taucher-Scholz G 2003 *Radiat. Res.* **159** 676–84
[52] Little J B 2006 *Health Phys.* **91** 416–26
[53] Morgan W F and Sowa M B 2007 *Mutat. Res.* **616** 159–64
[54] Mothersill C and Seymour C 2006 *Curr. Cancer Drug Targets* **6** 447–54
[55] Weber T J, Siegel R W, Markillie L M, Chrisler W B, Lei X C and Colburn N H 2005 *Mol. Carcinog.* **43** 31–7
[56] Yang H, Asaad N and Held K D 2005 *Oncogene* **24** 2096–103
[57] Yang H, Anzenberg V and Held K D 2007 *Radiat. Res.* **168** 292–8
[58] Azzam E I, de Toledo S M and Little J B 2003 *Oncogene* **22** 7050–7
[59] Fournier C, Becker D, Winter M, Barberet P, Heiss M, Fischer B, Topsch J and Taucher-Scholz G 2007 *Radiat. Res.* **167** 194–206
[60] Ward J F 2002 *Mutat. Res.* **499** 151–4
[61] Hu B, Wu L, Han W, Zhang L, Chen S, Xu A, Hei T K and Yu Z 2006 *Carcinogenesis* **27** 245–51
[62] Sokolov M V, Smilenov L B, Hall E J, Panyutin I G, Bonner W M and Sedelnikova O A 2005 *Oncogene* **24** 7257–65
[63] Fenech M, Chang W P, Kirsch-Volders M, Holland N, Bonassi S and Zeiger E 2003 *Mutat. Res.* **534** 65–75
[64] Medvedeva N, Ford J and Braby L 2004 *Radiat. Res.* **162** 660–6
[65] Ponnaiya B, Jenkins-Baker G, Brenner D J, Hall E J, Randers-Pehrson G and Geard C R 2004 *Radiat. Res.* **162** 426–32
[66] Belyakov O V, Malcolmson A M, Folkard M, Prise K M and Michael B D 2001 *Br. J. Cancer* **84** 674–9
[67] Shao C, Folkard M and Prise K M 2008 *Oncogene* **27** 434–40
[68] Kashino G, Prise K M, Schettino G, Folkard M, Vojnovic B, Michael B D, Suzuki K, Kodama S and Watanabe M 2004 *Mutat. Res.* **556** 209–15
[69] Shao C, Furusawa Y, Kobayashi Y, Funayama T and Wada S 2003 *FASEB J.* **17** 1422–7
[70] Hamada N, Ni M, Funayama T, Sakashita T and Kobayashi Y 2008 *Mutat. Res.* **639** 35–44
[71] Funayama T, Wada S, Kobayashi Y and Watanabe H 2005 *Radiat. Res.* **163** 241–6
[72] Schettino G, Folkard M, Prise K M, Vojnovic B, Held K D and Michael B D 2003 *Radiat. Res.* **160** 505–11
[73] Azzam E I, de Toledo S M and Little J B 2003 *Cancer Res.* **63** 7128–35
[74] Weyrather W K, Ritter S, Scholz M and Kraft G 1999 *Int. J. Radiat. Biol.* **75** 1357–64
[75] Heilmann J, Taucher-Scholz G, Haberer T, Scholz M and Kraft G 1996 *Int. J. Radiat. Oncol. Biol. Phys.* **34** 599–608
[76] Loebrich M, Cooper P K and Rydberg B 1998 *Radiat. Res.* **150** 619–26
[77] Stenerlöw B, Hoglund E, Carlsson J and Blomquist E 2000 *Int. J. Radiat. Biol.* **76** 549–57
[78] Kawata T, Durante M, Furusawa Y, George K, Ito H, Wu H and Cucinotta F A 2001 *Radiat. Res.* **156** 598–602
[79] Nasonova E, Ritter S, Gudowska-Nowak E and Kraft G 2001 *Phys. Med.* **17** (Suppl. 1) 198–201
[80] Fournier C and Taucher-Scholz G 2004 *Radiother. Oncol.* **73** (Suppl. 2) S119–22
[81] Goodhead D T 1994 *Int. J. Radiat. Biol.* **65** 7–17
[82] Krämer M and Kraft G 1994 *Adv. Space Res.* **14** 151–9

[83] Kanasugi Y, Hamada N, Wada S, Funayama T, Sakashita T, Kakizaki T, Kobayashi Y and Takakura K 2007 *Int. J. Radiat. Biol.* **83** 73–80
[84] Fournier C, Barberet P, Pouthier T, Ritter S, Fischer B, Funayama T, Hamada N, Kobayashi Y and Taucher-Scholz G 2008 *Radiat. Res.* submitted
[85] Nagasawa H and Little J B 1988 *Cancer Res.* **48** 4535–8
[86] Gault N, Rigaud O, Poncy J L and Lefaix J L 2007 *Radiat. Res.* **167** 551–62
[87] Tartier L, Gilchrist S, Burdak-Rothkamm S, Folkard M and Prise K M 2007 *Cancer Res.* **67** 5872–9
[88] Todd D G and Mikkelsen R B 1994 *Cancer Res.* **54** 5224–30
[89] Hino M, Wada S, Tajika Y, Morimura Y, Hamada N, Funayama T, Sakashita T, Kakizaki T, Kobayashi Y and Yorifuji H 2007 *Cell Struct. Funct.* **32** 51–6
[90] Belyakov O V, Mitchell S A, Parikh D, Randers-Pehrson G, Marino S A, Amundson S A, Geard C R and Brenner D J 2005 *Proc. Natl Acad. Sci. USA* **102** 14203–8
[91] Sedelnikova O A, Nakamura A, Kovalchuk O, Koturbash I, Mitchell S A, Marino S A, Brenner D J and Bonner W M 2007 *Cancer Res.* **67** 4295–302
[92] Jakob B, Rudolph J H, Gueven N, Lavin M F and Taucher-Scholz G 2005 *Radiat. Res.* **163** 681–90